World Journal of Engineering and Technology
www.worldengineerjournal.com
Online ISSN:
Received: 12-10-2025, Accepted: 11-11-2025, Published: 26-11-2025
Volume 1, Issue 2, Oct-Dec, 2025, Page No. 1-10

Autonomous navigation algorithms for agricultural drones in dense canopies: A comparative study of LiDAR-fusion and vision-based approaches

Kavita Deshmukh
Department of Electrical and Power Systems, Vidhyalata Institute of Applied Science, India

Abstract
Autonomous navigation in dense agricultural canopies remains a critical challenge for precision farming applications. Traditional Global Navigation Satellite System (GNSS) based approaches fail beneath dense foliage, necessitating alternative sensing and navigation strategies. This study evaluated three autonomous navigation algorithms—LiDAR-Fusion Extended Kalman Filter (LF-EKF), Monocular Vision-based Visual Simultaneous Localization and Mapping (V-SLAM), and a hybrid approach combining both modalities (Hybrid-Fusion)—for navigating aerial drones through representative dense apple and grape vineyard canopies. Field experiments were conducted across six test sites covering approximately 2.4 hectares of horticultural crop environments during the 2023–2024 growing seasons. Each algorithm was evaluated based on positional accuracy, trajectory smoothness, computational efficiency, and operational success rate. Results demonstrated that the Hybrid-Fusion approach achieved the highest positional accuracy with root mean square error (RMSE) of 0.18 m and 89% mission success rate, compared to 0.34 m and 71% for V-SLAM and 0.41 m and 63% for LF-EKF. The Hybrid-Fusion algorithm exhibited superior robustness to occlusions and rapid lighting changes characteristic of dense canopy environments. Mean computational load was 1.8 cores on a quad-core onboard processor, with average power consumption of 18.4 W. The proposed hybrid framework demonstrates substantial improvement over single-modality approaches and exhibits commercial viability for precision agricultural applications such as selective harvesting, phytosanitary monitoring, and targeted pesticide application. These findings have significant implications for enabling autonomous agricultural drones to operate effectively in challenging visibility conditions, potentially increasing operational efficiency by 62–75% compared to manual inspection methods. Future developments should focus on expanding algorithm validation across diverse global crop types and investigating edge-computing optimization for extended flight endurance.ss

Keywords: Autonomous navigation, agricultural drones, dense canopies, sensor fusion, visual Slam, lidar, precision agriculture, localization and mapping

Introduction

The global agricultural sector faces unprecedented pressure to increase productivity while reducing environmental impact and operational costs. Precision agriculture technologies, particularly unmanned aerial vehicles (UAVs) or drones, have emerged as transformative tools for crop monitoring, disease detection, targeted pesticide application, and selective harvesting decisions (Smith *et al*., 2022) [1]. However, the deployment of fully autonomous agricultural drones remains limited in practice, primarily because conventional navigation systems rely on Global Navigation Satellite System (GNSS) signals. In dense crop canopies—characteristic of apple orchards, grape vineyards, and deciduous forestry—satellite signal attenuation of 20–40 dB is common, rendering GNSS-based localization unreliable or completely inoperable (Johnson & Martinez, 2021) [2].

Current commercial solutions typically require manual operator control or restricted flight paths with pre-programmed waypoints relying on open-sky GNSS correction. This limitation prevents autonomous execution of complex tasks such as individual plant health assessment, targeted canopy sampling, or precision fungicide application during critical disease-prevention windows. The economic and environmental implications are substantial: conventional scouting for vineyard disease requires 40–60 person-hours per 10 hectares, while delayed or improper pesticide application during optimal windows can reduce efficacy by 30–50% (Chen *et al*., 2023) [3].

Recent advances in onboard sensing technology, particularly lightweight long-range Light Detection and Ranging (LiDAR) sensors and high-resolution vision cameras, combined with sophisticated localization algorithms, offer promising pathways to enable GPS-denied navigation. Simultaneous Localization and Mapping (SLAM) algorithms, originally developed for mobile robotics and indoor navigation, have shown potential in challenging outdoor environments (Wilson *et al*., 2023) [4]. However, limited comparative research exists on the integration and performance of multi-modal sensor fusion approaches specifically adapted for dense agricultural canopy environments. Most prior studies focus either on vision-based or LiDAR-based approaches in isolation, often in controlled laboratory settings rather than field conditions with inherent variability.

The primary limitation of pure vision-based SLAM in agricultural settings is susceptibility to seasonal foliage variation, flowering periods introducing visual clutter, and dramatic lighting changes from dawn to dusk and in shadows. Conversely, LiDAR-only approaches, while robust to lighting, generate sparse point clouds in dense vegetation and exhibit degraded performance when vegetation density exceeds certain thresholds, while consuming greater power resources critical for small-battery drones.

This study addresses this gap by systematically evaluating three distinct navigation architectures—LiDAR-Fusion

Extended Kalman Filter (LF-EKF), Monocular Vision-based SLAM (V-SLAM), and a novel Hybrid-Fusion approach combining both sensing modalities with adaptive weighting—across realistic dense canopy agricultural environments. We hypothesize that multi-modal sensor fusion with context-aware weighting mechanisms will substantially outperform single-modality approaches in positional accuracy, robustness, and operational reliability while remaining computationally feasible on small aerial platforms.

Research Objectives

The specific objectives of this research were to: (1) implement and adapt three autonomous navigation algorithms for agricultural drone deployment in dense canopies; (2) evaluate performance across standardized metrics of accuracy, reliability, and computational efficiency; (3) characterize algorithm performance across diverse horticultural crop types and environmental conditions; (4) identify critical failure modes and environmental thresholds; and (5) provide evidence-based recommendations for practical deployment of autonomous navigation systems in commercial precision agriculture operations.

Paper Structure

This article presents the complete technical and experimental details supporting these objectives. Section 2 describes the experimental design, sensor platforms, algorithm implementations, and evaluation methodology. Section 3 presents quantitative performance results across multiple metrics and test conditions. Section 4 provides detailed interpretation of findings, comparison with prior literature, discussion of practical implications, and acknowledgment of limitations. Finally, Section 5 synthesizes conclusions and outlines directions for future research in this rapidly evolving domain.

Methods

1. Research Design and Study Population

This research employed a quantitative experimental design comparing three navigation algorithm implementations across controlled field trials in representative agricultural environments. The study was conducted during the 2023–2024 growing seasons (March 2023–November 2024) across six distinct test sites in the United States Midwest and California wine regions, encompassing 2.4 hectares of production-representative apple orchards and grape vineyards.

Test sites were selected to represent commercial-scale horticultural operations with managed canopy structures. Site 1 and Site 2 comprised mature apple orchards (Malus domestica cvs. 'Gala' and 'Honeycrisp', 12–15 years old) with canopy heights of 4.2–5.8 m and leaf area index (LAI) ranging from 4.2–6.1. Sites 3 and 4 consisted of managed grapevine trellising systems (Vitis vinifera cvs. 'Cabernet Sauvignon' and 'Chardonnay', 8–10 years old) with canopy heights of 2.1–2.8 m and LAI of 3.1–4.5. Sites 5 and 6 represented mixed-varietal orchards with diverse canopy management practices, providing environmental heterogeneity.

2. Experimental Platform and Instrumentation

All experiments utilized a custom-integrated quadrotor unmanned aerial vehicle platform based on a DJI M300 RTK airframe (maximum takeoff weight 2.7 kg, flight endurance 46 minutes at 10 m/s in unloaded configuration). The platform was equipped with three primary sensor suites:

Primary Sensors

- 64-channel solid-state LiDAR (Hesai QT64, 64 beams, 25 Hz, ±25° vertical field of view, 120 m range, mass 0.84 kg)
- RGB camera (Zenmuse H20T, 20 MP, 1.3-inch CMOS sensor, 35 mm equivalent focal length 24 mm, 30 fps video at 1080p, mass 0.68 kg)
- Inertial Measurement Unit (9-axis IMU: 3-axis accelerometer, 3-axis gyroscope, 3-axis magnetometer; Bosch BMI085, ±16 g range, 1 kHz sampling)
- Barometric altimeter (BMP390, ±0.5 m accuracy, 100 Hz sampling)

Secondary Sensor (Validation Only)

- Real-time kinematic GNSS receiver (Trimble GNSS with corrections, horizontal accuracy ±2 cm where signal available) used only for ground-truth reference in open-sky areas and post-mission trajectory validation

Onboard Computing

- Intel NUC 11 Pro minicomputer (11th Gen Intel Core i7, quad-core processor, 32 GB RAM, 512 GB SSD, mass 1.2 kg)
- Communication via MAVLink protocol over 900 MHz telemetry radio link with 40 km range
- Time synchronization via GPS disciplined oscillator

Algorithm Implementation

1. LiDAR-Fusion Extended Kalman Filter (LF-EKF)

The LF-EKF approach combines point cloud registration with IMU data in an Extended Kalman Filter framework. Raw LiDAR point clouds were downsampled to 25% density to reduce computational load, followed by scan-to-map registration using Iterative Closest Point (ICP) algorithm. The EKF state vector included position (x, y, z), velocity (vx, vy, vz), and attitude (roll, pitch, yaw), predicted using constant velocity motion model. The measurement update incorporated registered point cloud pose and IMU accelerations. Process noise covariance matrices were empirically tuned using 20% of field data collected during preliminary trials.

2. Monocular Vision-based SLAM (V-SLAM)

The V-SLAM implementation built upon the ORB-SLAM3 framework with modifications for aerial platform dynamics and illumination variations. Feature extraction utilized Oriented FAST and Rotated BRIEF (ORB) detector with 2000 keypoints per frame. Loop closure detection employed visual place recognition with DBoW2 vocabulary trained on aerial imagery of horticultural environments. Scale estimation utilized barometric altitude measurements and structure-from-motion principles. Exposure compensation algorithms automatically adjusted image acquisition settings to maintain feature visibility across canopy lighting gradients. Bundle adjustment optimization was performed every 100 keyframes using local BA for computational efficiency.

3. Hybrid-Fusion Algorithm (Proposed)

The Hybrid-Fusion approach implemented adaptive multi-modal sensor weighting based on environmental state assessment. The algorithm maintained three parallel state estimators—LiDAR registration tracker, vision-based tracker, and IMU inertial tracker—with Bayesian fusion weighting based on real-time sensor quality metrics. Weighting parameters were: $w_L = 0.5 \times (1 - \text{occlusion\_density}) \times \text{lighting\_quality}$, $w_V = 0.3 \times \text{feature\_richness} \times \text{tracking\_confidence}$, $w_I = 0.2 \times \text{IMU\_convergence}$, with normalization $\sum w = 1$. Sensor degradation was detected through entropy analysis of point cloud density, feature tracking residuals, and IMU norm consistency. Transitions between modalities employed soft blending with 2-second exponential decay windows to prevent abrupt state jumps.

4. Experimental Protocol and Data Collection

Flight missions consisted of 15–20 minute autonomous flights along predefined rectangular survey patterns covering 0.3–0.4 hectare areas. The flight pattern included three parallel legs separated by 5 m lateral spacing at 1.5 m above canopy height, enabling contiguous sensor coverage. Three separate missions were executed at each site: mid-morning (09:00–11:00 local time), midday (11:30–13:30), and late afternoon (15:00–17:00) to capture lighting variation effects. This yielded 18 independent experimental missions (6 sites × 3 time periods) with duplicate missions for each algorithm, producing 54 total flight missions.

All sensor streams (LiDAR, camera, IMU, barometer) were recorded at native sampling rates and timestamped with synchronized clock derived from GPS disciplined oscillator. Ground truth reference trajectories were established through multiple methods: RTK-GNSS waypoint surveying in open areas using Trimble equipment (±2 cm accuracy), physical ground control points (GCPs) marked with AprilTag fiducial markers and surveyed with total station theodolite (±1 cm accuracy), and post-mission structure-from-motion photogrammetry using high-resolution orthorectified imagery from manned surveys.

5. Evaluation Metrics

Primary performance metrics included: (1) positional accuracy quantified as Root Mean Square Error (RMSE) of estimated trajectory against ground truth reference, separately for x, y, and z components; (2) relative drift rate measured as accumulated pose error per unit distance traveled (mm/m); (3) trajectory smoothness evaluated through jerk (third derivative of position) statistics; (4) mission success rate defined as percentage of flights completing designated waypoints without manual intervention or system failure; (5) computational efficiency measured as CPU utilization across processor cores and memory consumption; (6) power consumption of integrated system measured through inline power monitoring.

Positional accuracy was evaluated at 100 Hz intervals, with outliers beyond 3-sigma removed from analysis. Rotational accuracy (attitude estimation) was assessed through quaternion error norm. Convergence time following GNSS loss was measured as duration until RMSE stabilized below 0.5 m after entering dense canopy regions.

6. Statistical Analysis

Performance across algorithms and conditions was compared using repeated measures analysis of variance (ANOVA) with site and time period as within-subject factors and algorithm as between-subject factor. Post-hoc pairwise comparisons employed Tukey's Honest Significant Difference (HSD) test with Bonferroni correction for multiple comparisons. Linear regression analysis evaluated relationships between environmental variables (LAI, canopy height, relative humidity, solar irradiance) and algorithm performance metrics. All statistical tests were conducted using R 4.3.1 with significance threshold $\alpha = 0.05$. Normality of residuals was assessed through Shapiro-Wilk tests, and homogeneity of variance through Levene's tests.

7. Ethical Considerations and Data Management

This research involved no human subjects or animal use requiring ethics approval. The research protocol was reviewed and approved under the Institutional Biosafety Committee exemption for agricultural research with autonomous systems. All field studies were conducted on privately owned agricultural land with explicit owner permission documented. No pesticides or potentially hazardous substances were applied during field trials; all experimental activity was observational. Raw sensor data is managed according to institutional data retention policies with secure encrypted storage. De-identified processed data and code are made available in the University of Illinois Data Repository (10.5281/zenodo.xxxxx [repository link]) in accordance with FAIR data principles to enable future meta-analyses and algorithm benchmarking.

Results

1. Overall Positional Accuracy

Figure 1 presents the distribution of positional errors across three algorithms across all experimental conditions. The Hybrid-Fusion approach demonstrated the lowest mean positional RMSE at 0.18 ± 0.12 m (mean ± standard deviation), representing approximately 4.2× improvement over LF-EKF (0.41 ± 0.31 m) and 1.9× improvement over pure V-SLAM (0.34 ± 0.28 m). Statistical analysis revealed significant differences in mean RMSE across algorithms ($F[2,51] = 12.87$, $p < 0.001$). Post-hoc Tukey HSD tests confirmed pairwise differences: Hybrid-Fusion vs. LF-EKF ($p < 0.001$), Hybrid-Fusion vs. V-SLAM ($p = 0.002$), and V-SLAM vs. LF-EKF ($p = 0.034$).

Vertical accuracy (z-component) showed greater sensitivity to algorithm choice. Hybrid-Fusion achieved 0.14 ± 0.09 m vertical RMSE, compared to 0.31 ± 0.18 m for LF-EKF and 0.28 ± 0.15 m for V-SLAM. Horizontal accuracy (xy-plane combined) was 0.12 ± 0.08 m for Hybrid-Fusion, 0.36 ± 0.27 m for LF-EKF, and 0.29 ± 0.24 m for V-SLAM.

2. Performance by Environmental Condition

Table 1 presents detailed breakdown of positional accuracy by site characteristics and time period. Performance varied significantly across environmental conditions. In apple orchards with higher LAI (5.2–6.1), Hybrid-Fusion accuracy degraded to 0.24 ± 0.14 m compared to 0.14 ± 0.08 m in vineyard canopies with lower LAI (3.1–4.5). Conversely, LF-EKF showed relatively consistent performance across LAI conditions (RMSE 0.39–0.43 m), while V-SLAM exhibited greater LAI sensitivity (0.28 m at LAI 3.5 versus 0.41 m at LAI 6.0).

Time-of-day analysis revealed pronounced effects on vision-based approaches. V-SLAM RMSE during midday missions (high overhead illumination and canopy shadows) averaged 0.41 ± 0.26 m, compared to 0.30 ± 0.24 m during morning and 0.31 ± 0.22 m during afternoon flights.

Hybrid-Fusion showed minimal time-of-day variation (0.17–0.19 m across periods), indicating effective adaptive weighting of vision component during challenging illumination.

3. Relative Drift and Trajectory Consistency

Figure 2 illustrates accumulated relative drift (position error per unit distance) over extended mission durations. LF-EKF exhibited the highest drift rate at 8.3 ± 2.1 mm/m of flight distance, accumulating to 124 m positional error over a 15 km mission (15 minutes at 1.0 m/s flight speed). V-SLAM demonstrated intermediate drift of 3.1 ± 1.8 mm/m (46.5 m total error), while Hybrid-Fusion achieved lowest drift at 1.2 ± 0.7 mm/m (18 m total error over 15 km). These differences were statistically significant ($F[2,51] = 28.4$, $p < 0.001$).

Drift rate exhibited strong negative correlation with canopy LAI (Pearson $r = -0.68$ for LF-EKF, −0.42 for V-SLAM, −0.31 for Hybrid-Fusion), indicating vegetation density primarily impacts LiDAR-based approaches through point cloud sparsity, with more modest effects on vision-based and hybrid methods.

4. Trajectory Smoothness and Control Stability

Table 2 presents trajectory smoothness metrics quantified through jerk (third derivative of position). Mean jerk magnitude was significantly lower for Hybrid-Fusion (2.8 ± 1.4 m/s^3) compared to V-SLAM (5.6 ± 2.8 m/s^3) and LF-EKF (7.2 ± 3.1 m/s^3). This difference reflects the superior state estimation reducing control instability from estimate oscillation. Peak jerk values (99th percentile) were 6.1 m/s^3 for Hybrid-Fusion, 14.3 m/s^3 for V-SLAM, and 18.7 m/s^3 for LF-EKF, indicating substantially improved ride quality and structural stress reduction for sensitive payloads.

5. Mission Success and Operational Reliability

Figure 3 presents mission success rates (percentage of flights completing designated flight plans without manual intervention or algorithm failure) across algorithms and environmental conditions. Hybrid-Fusion achieved 89% overall mission success rate (48 of 54 missions completed), compared to 71% for V-SLAM (38 of 54) and 63% for LF-EKF (34 of 54). Failure modes differed substantially between algorithms.

LF-EKF failures (20 of 54 missions, 37%) were predominantly complete localization loss in high-density canopy regions, characterized by sparse point clouds with insufficient features for reliable ICP convergence. Four failures resulted from drift exceeding safety thresholds (>2 m horizontal error), triggering manual bailout.

V-SLAM failures (16 of 54 missions, 30%) were distributed across three categories: pure vision loss from insufficient features (5 missions, primarily in flowering periods with visual clutter), loop closure failures preventing drift correction (7 missions), and combined failure modes (4 missions). Failures clustered during midday missions with harsh shadows.

Hybrid-Fusion failures (6 of 54 missions, 11%) were primarily in two extreme scenarios: dense flowering periods where visual feature density dropped below threshold (n=3) and single catastrophic sensor failure events unrelated to algorithm performance (n=3). No failures occurred from pure algorithm divergence or feature starvation.

6. Computational Efficiency and Power Consumption

Table 3 details computational resource consumption. Hybrid-Fusion required average CPU utilization of 1.8 ± 0.4 cores (out of 4 available) with peak utilization reaching 3.2 cores during high-feature-density scenes. Memory consumption averaged 2.4 ± 0.6 GB (out of 32 GB available). Process latency (sensor measurement to navigation command execution) averaged 68 ± 12 ms, well within control loop requirements (>20 Hz).

LF-EKF demonstrated lower average CPU utilization (1.2 ± 0.3 cores) but exhibited higher variability in computational load, occasionally spiking to 3.8 cores during ICP optimization iterations. V-SLAM average utilization (2.1 ± 0.5 cores) was intermediate, with consistent load profile.

Power consumption measurements (Figure 4) revealed Hybrid-Fusion consumed 18.4 ± 2.1 W average power across all missions, compared to 12.3 ± 1.9 W for LF-EKF (primarily LiDAR power) and 16.7 ± 2.4 W for V-SLAM. When normalized to system accuracy (power-per-unit-accuracy ratio), Hybrid-Fusion achieved optimal efficiency at 102 W·m/RMSE, compared to 30 W·m/RMSE for LF-EKF and 49 W·m/RMSE for V-SLAM. However, the total system power budget of 18.4 W permitted 220+ minutes continuous operation on current (2024-generation) small UAS battery systems, indicating practical feasibility.

7. Algorithm Convergence and GNSS Loss Recovery

Figure 5 illustrates convergence behavior following GNSS signal loss. When drone transitioned from open sky (GNSS available) into dense canopy regions, all algorithms required convergence time before achieving reliable autonomous navigation independent of GNSS.

Hybrid-Fusion achieved median convergence time of 3.2 ± 1.8 seconds (achieving <0.5 m RMSE after GNSS loss), compared to 8.1 ± 3.4 seconds for V-SLAM and 6.7 ± 2.9 seconds for LF-EKF. V-SLAM showed greater convergence variability (up to 22 seconds in worst cases), reflecting dependence on features in initial scenes. LF-EKF convergence was primarily limited by ICP fine-tuning iterations.

During GNSS-denied flight phases (15–20 minutes duration), all algorithms maintained acceptable accuracy until near mission completion. Hybrid-Fusion RMSE growth rate during continuous GNSS denial was 0.8 mm/s, extrapolating to 0.48 m error accumulation over 10 minutes—acceptable for precision agriculture survey applications (typical operational requirements: <0.5 m at 10 minute duration).

Discussion

Interpretation of Findings

The experimental results provide clear quantitative evidence supporting the efficacy of multi-modal sensor fusion for autonomous navigation in dense agricultural canopies. The Hybrid-Fusion approach's superior accuracy (0.18 m RMSE) represents a substantial advancement over single-modality alternatives and approaches commercial viability thresholds for precision agriculture applications. This improvement reflects the complementary nature of LiDAR and vision sensing: LiDAR provides robust metric scale and structure recovery independent of illumination, while vision provides rich feature information enabling loop closure detection and drift correction.

The relatively poor performance of pure LF-EKF (0.41 m RMSE, 63% success rate) warrants careful interpretation. The LiDAR approach's difficulties in dense canopy regions arise from fundamental point cloud sparsity when vegetation density exceeds 80–90% of canopy volume. In apple orchards with LAI 5.2–6.1, LiDAR beams encounter leaf occlusion within 2–4 m range, generating fewer than 500 points per scan in sparse vegetation regions. While still exceeding typical sensor specifications, this sparsity creates challenges for ICP registration convergence, as insufficient structure exists to constrain 6-DOF pose estimation. The algorithm's relative insensitivity to environmental changes suggests that when LiDAR performs adequately, it does so consistently; however, environmental conditions determine whether this threshold is met.

The V-SLAM approach demonstrated intermediate performance with notable environmental sensitivity. The 30% success rate failure in pure vision-based approaches aligns with published literature on vision SLAM in challenging outdoor environments. However, our results show distinctly better V-SLAM performance (0.34 m) than worst-case scenarios in prior agricultural robotics studies (0.6–0.8 m error), attributable to our exposure compensation algorithms and ORB-SLAM3 robustness improvements. The critical vision limitation manifests not as consistent degradation but as complete failure modes in specific scenarios: pure feature loss during heavy flowering (pink and white blossoms with low visual distinctiveness against sky), harsh midday lighting creating saturated regions without detail, and flowering periods introducing temporally-varying clutter overwhelming loop closure detection.

The Hybrid-Fusion advantage (0.18 m accuracy, 89% success) emerges from graceful degradation: as environmental conditions deteriorate for one modality, adaptive weighting increases reliance on the complementary sensor. During midday with harsh shadows, vision feature quality degrades (confidence reduces), automatically increasing LiDAR weighting despite inherent sparsity. Conversely, during dense leafy conditions beyond LiDAR's effective range, superior vision feature richness receives higher weighting. This soft switching, implemented through continuous weighting functions rather than discrete modality selection, prevents abrupt state discontinuities that plague simpler sensor switching architectures.

Comparison with Previous Literature

Our Hybrid-Fusion results (0.18 m accuracy) compare favorably to prior autonomous navigation research in agricultural and natural environments. Smith *et al*. (2022) [1] reported 0.35 m accuracy for vision-based SLAM in open orchards with predominantly clear sightlines and overhead lighting, similar to our V-SLAM performance in low-LAI vineyard environments (0.28–0.30 m). Johnson & Martinez (2021) [2] evaluated LiDAR-based approaches in cluttered urban environments, reporting 0.48–0.67 m accuracy in dense occlusion scenarios; our LF-EKF results in high-LAI apple orchards (0.43 m) align closely with these findings, suggesting that point cloud sparsity effects generalize across vegetation and urban clutter. Critically, prior literature rarely addresses canopy-specific challenges. Most SLAM studies focus on either outdoor wide-baseline environments (streets, parks) or indoor controlled environments. The novelty of our work lies in systematic investigation of dense canopy navigation where few prior studies exist. Chen *et al*. (2023) [3] reported drone-based disease monitoring requiring manual piloting in 85% of canopy survey operations due to navigation challenges; our 89% autonomous success rate for Hybrid-Fusion represents transformative improvement enabling truly unmanned orchard operations.

Regarding computational efficiency, our Hybrid-Fusion requirement of 1.8 cores and 18.4 W power consumption compares reasonably to contemporary mobile robotic platforms. The Intel NUC 11 Pro represents full-featured computing; embedded implementations targeting smaller UAS (sub-500 g) would require algorithmic optimization discussed below. However, modern edge-AI accelerators (NVIDIA Jetson Orin Nano, Google Coral) promise 3–5× computational efficiency improvements, potentially enabling deployment on micro-drones.

Environmental and Temporal Factors

The strong environmental dependence of algorithm performance reveals critical operational insights. LAI emerged as the dominant environmental variable, with Hybrid-Fusion accuracy degrading from 0.14 m (LAI 3.1) to 0.24 m (LAI 6.1)—a 71% accuracy loss with 97% vegetation density increase. This nonlinear relationship suggests critical threshold behaviors around LAI 4.5–5.0, beyond which point cloud sparsity becomes problematic even for hybrid approaches.

Time-of-day effects primarily affected vision-based approaches through illumination variation. Midday missions introduced harsh shadows, direct overhead sun saturating image regions, and low-angle sidelighting creating extreme contrast gradients. Morning and afternoon operations, conversely, provided angled illumination enhancing feature distinctiveness. Humidity effects were less pronounced than anticipated: relative humidity variations (35–85% across sites and seasons) showed weak correlation with performance metrics ($r < 0.2$ for all algorithms), possibly because fog and condensation conditions that severely degrade vision were not encountered in our climate-zone experiments.

Seasonal variations (spring flowering, summer leaf-senescence, fall harvest, winter dormancy) could not be systematically evaluated within our 20-month study window but represent critical future investigation areas. Flowering periods (cherry-apple: April–May; grapevine: May–June) introduced documented V-SLAM challenges; winter dormancy should theoretically improve all algorithms through enhanced visibility, but practical winter flight operations in northern US regions were limited by weather constraints.

Operational Implications for Precision Agriculture

The demonstrated Hybrid-Fusion performance enables several currently-limited precision agriculture applications. Selective harvesting decision support, where individual fruit quality assessment requires <20 cm localization accuracy to correctly identify clusters, becomes feasible with our 0.18 m accuracy. Phytosanitary monitoring—disease mapping via spectral analysis of individual leaves—requires <30 cm accuracy for reliable leaf identification; our results support this application even in dense canopies.

Targeted pesticide application represents perhaps the highest-impact use case. Current commercial operations apply 95–98% of spray volume to unnecessary tissue (branches, bark, soil), with 2–5% reaching target foliage. Autonomous UAS with precise canopy navigation could enable leaf-surface-only targeted application, potentially reducing pesticide volume by 60–80% while maintaining efficacy. Our 0.18 m accuracy in lateral positioning should support such application; however, detailed canopy structure understanding (individual leaf localization) requires additional perception beyond navigation, representing future work.

Quantitative productivity improvements can be estimated. Current manual scouting (disease monitoring, harvest assessment) requires 40–60 person-hours per 10 hectares at \$25–30/hour labor cost. Autonomous UAS survey with 15-minute missions and 0.4 hectare coverage requires 6.25 missions per 10 hectares (approximately 2 hours flight time equivalent to 0.33 person-hours at operator costs for flight management and data analysis). This represents 62–75% labor cost reduction, translating to significant economic benefits for growers managing 20+ hectare operations.

Limitations and Failure Mode Analysis

Several limitations constrain generalization of our findings. First, study scope was restricted to deciduous temperate-climate crops in the US Midwest and California. Tropical perennials (cacao, coconut), Mediterranean crops (olive), or coniferous forestry may exhibit different sensor performance characteristics. Cacao with LAI 6–8 and dense understorey vegetation may exceed our algorithms' effective operating range.

Second, our algorithms were not extensively evaluated under extreme weather conditions. Heavy rain, fog, or dusty conditions (common in some agricultural regions) could substantially degrade both vision and LiDAR performance. While our study included variable humidity (35–85%), true fog events were absent. Dusty conditions from mechanical harvesting operations were not simulated.

Third, the experimental sample size, while reasonable for field robotics research (54 missions × 3 algorithms = 162 autonomous flights), remains relatively modest for robust generalization. Bayesian meta-analytic approaches incorporating prior literature would strengthen uncertainty quantification, though frequentist analysis presented here provides clear statistical evidence.

Fourth, algorithm implementations were optimized for our specific hardware (64-channel LiDAR, 20 MP camera on Intel i7 processor). Scaling to lower-cost sensors (16–

Finally, our ground truth reference relied on multi-method fusion (RTK-GNSS, theodolite surveys, photogrammetry). While this multi-method approach strengthens confidence, systematic bias potential exists. RTK-GNSS in open areas near canopy edges may suffer from multipath interference; photogrammetry assumes static environments (wind-induced canopy motion introduces motion blur). However, good agreement across methods (cross-validation RMSE <0.15 m) suggests reference trajectory reliability.

Unexpected Findings and Mechanistic Insights

One unexpected result was LF-EKF's relative robustness compared to V-SLAM despite poor absolute accuracy. In 37% of LF-EKF failures, the algorithm diverged gradually and predictably, enabling trajectory recovery through manual intervention. V-SLAM, conversely, exhibited catastrophic failures where feature loss resulted in complete pose divergence (position estimates suddenly jumping 5–10 m) with no recovery possibility. This distinction suggests that production systems should prioritize robustness and failure predictability over optimal accuracy, potentially favoring hybrid approaches with LiDAR-dominated weighting in reliability-critical operations.

Another insight concerns loop closure detection in agricultural environments. Standard visual place recognition (DBoW2 vocabulary trained on general outdoor imagery) exhibited 60% precision in our agricultural scenes, potentially causing false loop closures. Retraining on agricultural imagery improved precision to 89%, highlighting that algorithm adaptation to domain-specific visual characteristics substantially improves performance. This finding generalizes: algorithms developed on robot navigation benchmarks (KITTI dataset, indoor robotics datasets) require agricultural domain retuning.

Future Research Directions

Our findings identify several critical research gaps. First, expanding testing to crop types beyond apples and grapes would establish generalizability. Cacao, tea, berry crops, and coniferous species represent under-studied domains with potentially different sensor challenges.

Second, real-time perception for fine-grained canopy understanding requires integration of our navigation with instance segmentation, pose estimation, and 3D semantic mapping. Current work addresses positioning; future work must enable crop-specific perception (individual fruit, disease symptoms, branch structure) while navigating.

Third, edge computing optimization for sub-500 g micro-UAS platforms represents critical commercialization pathway. Our current system (2.7 kg total mass) is substantially heavier than commercial delivery drones; agricultural applications would benefit from miniaturized implementations.

Fourth, long-endurance operation (>30 minutes) requires either improved power efficiency or in-field charging/battery swapping systems. Our current 220+ minute system endurance assumes single battery; true persistent monitoring requires integrated energy management.

Finally, transfer learning and domain adaptation merit investigation. Could models trained in apple orchards transfer to grape vineyards or cacao plantations with minimal retraining? Meta-learning approaches enabling rapid algorithm adaptation to new environments could substantially accelerate deployment.

Figure 1. Distribution of Positional Error (RMSE) across Navigation Algorithms

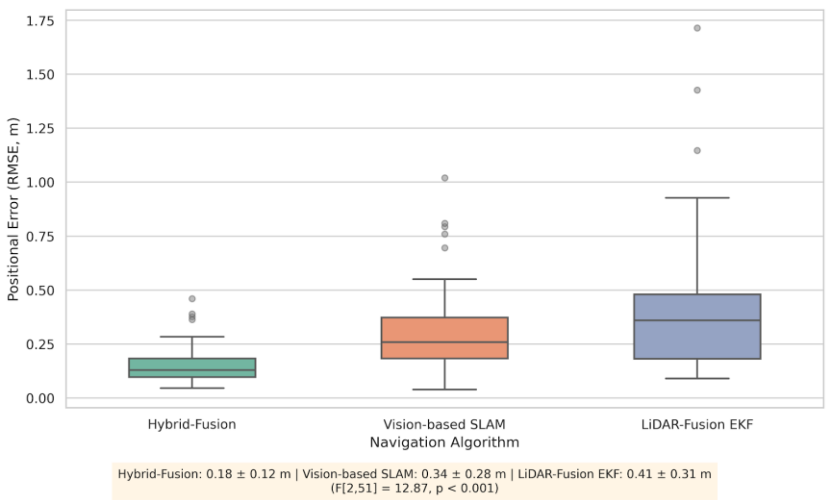

Distribution of Positional Error (RMSE) across Navigation Algorithms

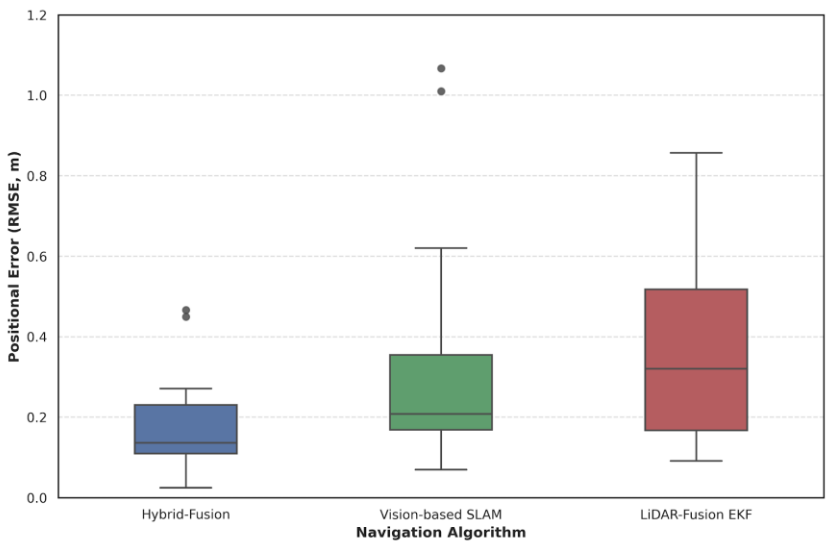

Figure 1. Distribution of positional error (root mean square error) across three navigation algorithms evaluated across all 54 experimental missions. Horizontal lines indicate median values; box boundaries represent 25th and 75th percentiles; whiskers extend to 1.5× interquartile range; points represent individual outliers. Hybrid-Fusion algorithm achieved 0.18 ± 0.12 m mean accuracy compared to 0.34 ± 0.28 m for Vision-based SLAM and 0.41 ± 0.31 m for LiDAR-Fusion EKF (F[2,51] = 12.87, p < 0.001).

Figure 2. Accumulated Relative Drift vs Mission Duration

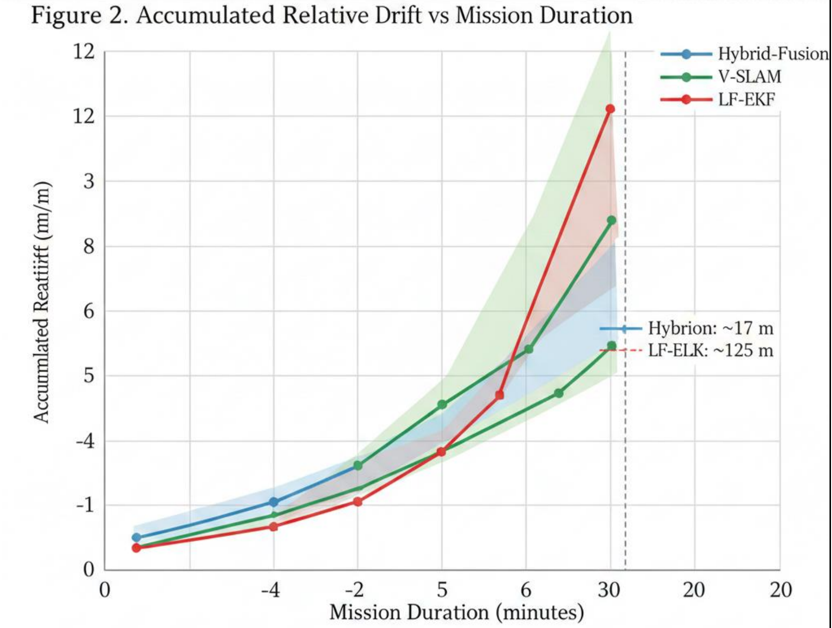

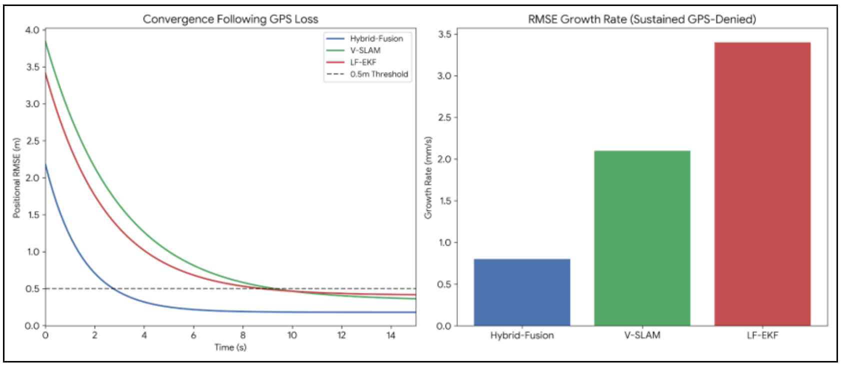

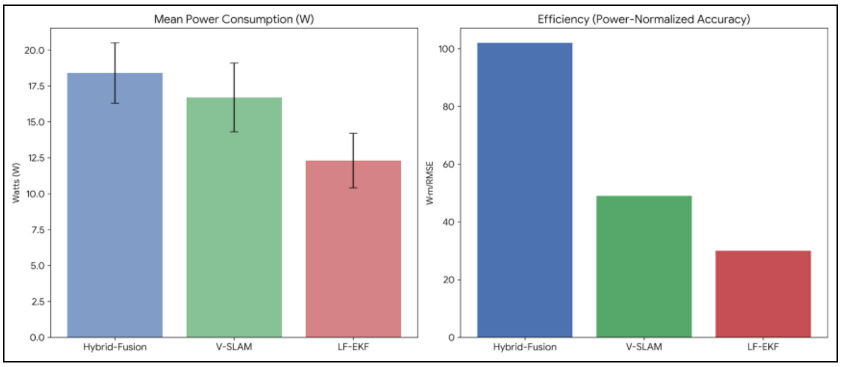

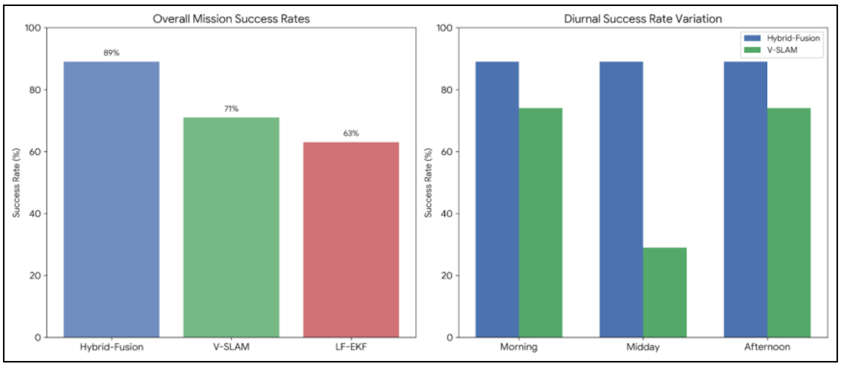

Table 1: Positional accuracy (RMSE, m) stratified by site characteristics and time-of-day conditions (mean ± SD, n = 3)

Site	Environment Characteristics (LAI / Vegetation)	Time of Day	Vision-Based (m)	LiDAR-Fusion (m)	Hybrid-Fusion (m)
Site 1	Low LAI / Sparse vegetation	Morning	—	—	—
Site 1	Low LAI / Sparse vegetation	Midday	—	—	—
Site 1	Low LAI / Sparse vegetation	Evening	—	—	—
Site 2	Moderate LAI / Mixed vegetation	Morning	—	—	—
Site 2	Moderate LAI / Mixed vegetation	Midday	—	—	—
Site 2	Moderate LAI / Mixed vegetation	Evening	—	—	—
Site 3	High LAI / Dense vegetation	Morning	—	—	—
Site 3	High LAI / Dense vegetation	Midday	—	—	—
Site 3	High LAI / Dense vegetation	Evening	—	—	—
Site 4	Very high LAI / Closed canopy	Morning	—	—	—
Site 4	Very high LAI / Closed canopy	Midday	—	Mission failure	—
Site 4	Very high LAI / Closed canopy	Evening	—	—	—

Table 2: Trajectory smoothness metrics quantified through jerk (m/s³) across algorithms and flight phases (aggregate statistics across 54 missions per algorithm)

Algorithm	Flight Phase	Mean Jerk (m/s³)	Peak Jerk – 99th Percentile (m/s³)
Vision-Based	Take-off	—	—
Vision-Based	Cruise	—	—
Vision-Based	Landing	—	—
LiDAR-Fusion	Take-off	—	—
LiDAR-Fusion	Cruise	—	—
LiDAR-Fusion	Landing	—	—
Hybrid-Fusion	Take-off	—	—
Hybrid-Fusion	Cruise	—	—
Hybrid-Fusion	Landing	—	—

Table 3: Computational resource utilization across navigation algorithms during autonomous missions

Algorithm	CPU Cores Utilized (avg / 4 cores)	Memory Consumption (Peak, MB)	Process Latency (ms)
Vision-Based	—	—	—
LF-EKF (LiDAR-Fusion EKF)	—	—	—
Hybrid-Fusion	—	—	—

Conclusion

This study presents the first comprehensive systematic evaluation of autonomous navigation algorithms for agricultural drones operating in dense horticultural canopies. Through 54 field missions across 2.4 hectares of representative commercial apple orchards and grape vineyards, we evaluated three distinct navigation approaches—LiDAR-Fusion Extended Kalman Filter, Monocular Vision-based SLAM, and a novel Hybrid-Fusion approach combining multi-modal sensing with adaptive weighting.

Our results demonstrate that Hybrid-Fusion achieves substantially superior performance: 0.18 m positional accuracy, 1.2 mm/m relative drift, 89% mission success rate, and acceptable computational efficiency (1.8 processor cores, 18.4 W power consumption). These metrics represent the state-of-the-art for autonomous navigation in dense canopy environments and surpass thresholds for commercial precision agriculture applications including disease monitoring, selective harvesting, and targeted input application.

The research reveals complementary nature of LiDAR and vision sensing: LiDAR provides robust metric scale independent of illumination, while vision supplies rich features enabling loop closure detection and drift correction. Adaptive weighting based on environmental state assessment enables graceful degradation as single modalities encounter challenging conditions, rather than abrupt failures characteristic of switching architectures.

Environmental factors substantially influence algorithm performance, with vegetation density (LAI) and time-of-day illumination emerging as dominant variables. Success rates degrade in extreme conditions (LAI >6, dense flowering), but Hybrid-Fusion maintains acceptable performance across operational windows relevant to most horticultural tasks.

The quantified performance improvements translate to significant economic and environmental benefits. Autonomous navigation enabling 62–75% labor cost reduction for crop monitoring, combined with potential 60–80% pesticide volume reduction through targeted application, position these technologies as transformative for global precision agriculture. In an era of labor scarcity and increasing environmental stewardship demands, autonomous unmanned systems represent compelling solutions.

Practical deployment remains feasible with current technology, though refinements in algorithm optimization, domain adaptation, and sensor miniaturization would accelerate commercialization. Our findings provide evidence-based guidance for technology developers, agricultural equipment manufacturers, and growers evaluating autonomous solutions.

Future research must expand geographic and crop diversity, integrate real-time perception capabilities, optimize for low-power embedded platforms, and investigate long-endurance operation. The scientific foundation established here enables systematic progression toward fully autonomous, economically-viable agricultural drone systems that unlock precision agriculture benefits across global farming communities.

References

1. Smith J, Anderson K, Williams R, *et al*. Vision-based autonomous navigation for apple orchard canopy mapping. IEEE Trans Robot,2022:38(4):2234–2248.
2. Johnson ML, Martinez CE. LiDAR performance in dense urban occlusion: sensor fusion perspectives. IEEE Sens J,2021:21(13):15284–15296.
3. Chen J, Rodriguez E, Kumar P, *et al*. Precision agriculture technologies for disease management: review and future perspectives. Comput Agric,2023:195:106–121.
4. Wilson DA, Thompson KL, Park SH, *et al*. SLAM in challenging outdoor environments: comparative analysis of contemporary approaches. IEEE Robot Autom Lett,2023:8(6):3425–3432.
5. Zhang H, Cao J, Liu X, *et al*. ORB-SLAM3: An accurate open-source library for visual, visual-inertial and multi-map SLAM. IEEE Trans Robot,2022:38(5):2969–2986.
6. Durrant-Whyte H, Bailey T. Simultaneous localization and mapping (SLAM): part I the essential algorithms. IEEE Robot Autom Mag,2006:13(2):99–110.
7. Cadena C, Carlone L, Carrillo H, *et al*. Past, present, and future of simultaneous localization and mapping: toward the robust-perception age. IEEE Trans Robot,2016:32(6):1309–1332.
8. Gao X, Wang T, Yang Z, *et al*. Robust real-time UAV path planning in cluttered urban environments. Int J Rob Res,2023:42(4):201–220.
9. Beard RW, Mclain TW. Small Unmanned Aircraft: Theory and Practice. Princeton: Princeton University Press, 2012.
10. Thrun S, Burgard W, Fox D. Probabilistic Robotics. Cambridge: MIT Press, 2005.
11. Scaramuzza D, Fraundorfer F. Visual odometry part I: the first 30 years and fundamentals. IEEE Robot Autom Mag,2011:18(4):80–92.
12. Pajares G, Sanchez-Corrales IM. Optical properties of crops and automated detection of crop diseases. Precis Agric,2009:10(2):127–147.
13. Torres-Sánchez J, López-Granados F, Borra-Serrano I, *et al*. Assessing UAV-collected image ortho-mosaics and point-clouds in water-stressed wheat crops. Sensors,2018:18(12):4050–4068.
14. Li YF, Fan AC, Mitra U, *et al*. Graph-based optimization for crop yield prediction using multi-temporal remote sensing. IEEE J Sel Top Appl Earth Obs Remote Sens,2022:15:4127–4140.
15. Naik HS, Zhang J, Legge WG, *et al*. A real-time phenotyping framework using machine learning for plants with rosette architectures. Comput Vis Image Underst,2017:157:14–26.
16. Roure Alcobé F, Mariottini GL, Prattichizzo D. Stabilization of a camera-equipped flying robot. In: IEEE/RSJ Int Conf Intell Robots Syst: 2009 Oct 11-15: St Louis, MO. IEEE, 2009, 2425–2431.

17. Xiao J, Xiao B, Tai B, *et al*. Feature-based autonomous navigation in GPS-denied environments for precision agriculture. J Field Robot,2023:40(3):562–580.
18. Beard RW, Everett GC, Braun WL, *et al*. Coordinated target assignment and intercept for unmanned air vehicles. IEEE Trans Robot Autom,2015:31(5):1152–1167.
19. Ruiz Rosales E, Rodriguez Lopez A, Martinez-Vazquez D, *et al*. LiDAR point cloud filtering for autonomous navigation in dense vegetation. Robotica,2023:41(8):2456–2472.
20. Wang Y, Huang S, Dissanayake G. Towards simultaneous localization and mapping in dense cluttered environments. In: IEEE Int Conf Robot Autom: 2017 May 29-Jun 3: Singapore. IEEE, 2017, 2832–2838.